JOURNAL OF GEOPHYSICAL RESEARCH: SPACE PHYSICS, VOL. 118, 2783–2788, doi:10.1002/jgra.50325, 2013

Neutron monitor yield function: New improved computations

A. L. Mishev,[1,3] I. G. Usoskin,[1,2] and G. A. Kovaltsov[4]

Received 15 November 2012; revised 12 April 2013; accepted 7 May 2013; published 6 June 2013.

[1] A ground-based neutron monitor (NM) is a standard tool to measure cosmic ray (CR) variability near Earth, and it is crucially important to know its yield function for primary CRs. Although there are several earlier theoretically calculated yield functions, none of them agrees with experimental data of latitude surveys of sea-level NMs, thus suggesting for an inconsistency. A newly computed yield function of the standard sea-level 6NM64 NM is presented here separately for primary CR protons and α-particles, the latter representing also heavier species of CRs. The computations have been done using the GEANT-4 PLANETOCOSMICS Monte-Carlo tool and a realistic curved atmospheric model. For the first time, an effect of the geometrical correction of the NM effective area, related to the finite lateral expansion of the CR induced atmospheric cascade, is considered, which was neglected in the previous studies. This correction slightly enhances the relative impact of higher-energy CRs (energy above 5–10 GeV/nucleon) in NM count rate. The new computation finally resolves the long-standing problem of disagreement between the theoretically calculated spatial variability of CRs over the globe and experimental latitude surveys. The newly calculated yield function, corrected for this geometrical factor, appears fully consistent with the experimental latitude surveys of NMs performed during three consecutive solar minima in 1976–1977, 1986–1987, and 1996–1997. Thus, we provide a new yield function of the standard sea-level NM 6NM64 that is validated against experimental data.

Citation: Mishev, A. L., I. G. Usoskin, and G. A. Kovaltsov (2013), Neutron monitor yield function: New improved computations, *J. Geophys. Res. Space Physics*, *118*, 2783–2788, doi:10.1002/jgra.50325.

1. Introduction

[2] The Earth is constantly bombarded by energetic particles—cosmic rays (CRs), which consist of nuclei of various elements, mostly protons and α-particles. The lower energy part (below several tens of GeV/nucleon) of the galactic CR (GCR) energy spectrum is modulated in the solar wind and the heliospheric magnetic field which are ultimately related to solar activity [e.g., *Potgieter*, 1998]. The main instrument to study the CR variability is the world network of neutron monitors (NMs) [*Shea and Smart*, 2000; *Moraal et al.*, 2000]. A NM [*Simpson*, 1958] is an instrument that provides continuous recording of the hadron component of atmospheric secondary particles [*Hatton*, 1971], which is related to the intensity of high-energy primary nuclei impinging on the Earth's atmosphere from space. The purpose of the NM is to detect variations of intensity in the interplanetary CR spectrum. A major challenge is the reconstruction of primary particle characteristics from ground-based data records, since the NM is an energy-integrating device measuring only the secondaries (mainly protons and neutrons) deep in the atmosphere. The task of linking NM count rates to the intensity of primary CRs is non-trivial and requires extensive numerical simulations of the atmospheric cascade, initiated by energetic CR [e.g., *Clem and Dorman*, 2000]. A standard way to do it is to calculate the NM yield function, viz. response of a standard NM to the unit intensity of primary CR particles with fixed energy.

[3] Several attempts have been performed to calculate the NM yield function. Because of the complexity of atmospheric cascades, Monte-Carlo simulation provides the most useful tool to calculate the yield function. *Debrunner et al.* [1982] used a state-of-the-art specifically developed Monte-Carlo simulation of the atmospheric cascade [*Debrunner and Brunberg*, 1968]. *Clem and Dorman* [2000] applied the FLUKA Monte-Carlo package for the simulations. *Matthiä* [2009], *Matthiä et al.* [2009], and *Flückiger et al.* [2008] used the GEANT-4 Monte-Carlo package. Because of the different model assumptions (hadron interaction models, atmospheric models, and numerical schemes), the results are somewhat different (within 10–15%) between different packages [*Heck*, 2006; *Bazilevskaya et al.*, 2008]. While a NM is a standard device, the local surrounding may vary quite a bit for individual NMs (efficiency of the

[1]Sodankylä Geophysical Observatory (Oulu unit), University of Oulu, Oulu, Finland.
[2]Department of Physics, University of Oulu, Finland.
[3]Institute for Nuclear Research and Nuclear Energy, Bulgarian Academy of Sciences, Sofia, Bulgaria.
[4]Ioffe Physical-Technical Institute of Russian Academy of Sciences, St. Petersburg, Russia.

Corresponding author: I. Usoskin, Sodankylä Geophysical Observatory (Oulu unit), University of Oulu, Oulu, Finland. (Ilya.Usoskin@oulu.fi)

2169-9380/13/10.1002/jgra.50325

This article was corrected on 31 OCT 2016. See the end of the full text for details.

Table 1. Yield Function (in Units of [m^2 sr]) of the Standard 6NM64 Sea-Level Neutron Monitor for the Primary Protons (Columns 2–3) and α-Particles (Columns 5–6), Per Nucleon of the Primary Particle

Protons			α-Particles		
P (GV)	E_p (GeV)	Y_p	P (GV)	E_α (GeV/nuc)	Y_α
0.7	0.232	$7.26 \cdot 10^{-9}$			
1	0.433	$8.46 \cdot 10^{-6}$	3.38	1	$3.86 \cdot 10^{-4}$
2	1.27	$1.21 \cdot 10^{-3}$	5.55	2	$2.16 \cdot 10^{-3}$
3	2.21	$5.42 \cdot 10^{-3}$	7.64	3	$4.31 \cdot 10^{-3}$
4	3.17	$9.43 \cdot 10^{-3}$	9.69	4	$7.27 \cdot 10^{-3}$
5	4.15	0.02	11.7	5	$1.18 \cdot 10^{-2}$
10	9.11	0.109	21.8	10	$8.37 \cdot 10^{-2}$
20	19.1	0.229	41.8	20	0.215
50	49.1	0.59	100	49.1	0.59
100	99.1	0.992	200	99.1	0.992
500	499.1	3.35	1000	499.1	3.35
1000	999.1	6.67	2000	999.1	6.67

detection system and local environment [e.g., *Krüger et al.*, 2008]), which may cause deviation of ±15% from the "standard" unit [*Usoskin et al.*, 2005]. Therefore, it is hardly possible to directly calibrate the yield function for a given NM and define which one is more correct.

[4] However, there is an indirect way to test the NM yield function, via latitude surveys [*Clem and Dorman*, 2000; *Caballero-Lopez and Moraal*, 2012]. During a sea-level latitude survey, an NM is placed onboard a ship which scans all geomagnetic latitudes, from the equator to the polar region. Accordingly, the measured count rate can be calculated via the geomagnetic shielding and the yield function of a NM and assuming the constant primary CR intensity during the survey. For the latter, surveys are typically done during periods of solar minima. Moreover, the local environment remains constant during the cruise. A number of NM latitude surveys have been performed in the past [*Potgieter et al.*, 1979; *Moraal et al.*, 1989; *Villoresi et al.*, 2000] to provide a basis to validate the NM yield function. *Caballero-Lopez and Moraal* [2012] have made a detailed analysis of experimental data and demonstrated that none of the previously theoretically calculated yield functions can reproduce the observed latitude surveys. This was ascribed primarily to the potential role of obliquely incident primary CR particles [*Clem and Dorman*, 2000]. All the theoretically calculated earlier yield functions predict too strong latitudinal dependence of the NM count rate compared to the observed one, suggesting that the contribution of higher energy CRs is somewhat underestimated in the models compared to the lower energy part.

[5] In order to resolve the situation, *Caballero-Lopez and Moraal* [2012] presented an empirically derived NM yield function, which is the derivative of an NM latitude survey de-convoluted with the prescribed energy spectrum of GCR. This empirical approach, while fixing the discrepancy related to latitude surveys, has however its own weak point—the high rigidity (above 16–17 GV, which is the vertical geomagnetic cutoff rigidity at the magnetic equator) tail of the thus defined yield function is based solely on an extrapolation of the latitude survey, Thus, this empirically based ad-hoc yield function remains unclear for the energy range above this rigidity/energy range, which is responsible for half or more of the NM count rate [*Ahluwalia et al.*, 2010]. Moreover, this method is slightly model dependent and cannot distinguish yields for protons and α-particles. Thus, there is still a crucial need for a theoretical updated computation of the NM yield function that would agree with the experimental data.

[6] Here we present a new, improved computation of the yield function of a standard 6NM64 NM. In our model, we considered an effect neglected in previous theoretical computations of the yield function—increase of the effective area of an NM as function of the energy of primary CR due to lateral extent of the atmospheric cascade for high-energy particles. This effect is responsible for higher, than earlier though, response of an NM to high-energy CRs and, as a consequence, leads to perfect agreement with the measured latitude surveys.

[7] In section 2, we describe the detail of the NM yield function computation. The newly computed NM yield function is presented in Table 1 and Figure 3, and confronted with the measured latitude surveys in section 3. Conclusions are given in section 4.

2. Computation of the NM Yield Function

[8] The total response of a NM to CRs can be determined by convolution of the CR spectra with the yield function. The count rate of a NM at time t is presented as:

$$N(P_c, h, t) = \sum_i \int_{P_c}^{\infty} Y_i(P, h) J_i(P, t) dP \qquad (1)$$

where P_c is the local geomagnetic cutoff rigidity [*Smart et al.*, 2006], h is the atmospheric depth (or altitude). The term $Y_i(P,h)$ [m^2 sr] represents the NM yield function for primaries of particle type i, $J_i(P,t)$ [GV m^2 sr s]$^{-1}$ represents the rigidity spectrum of primary particle of type i at time t. The NM yield function is defined as [e.g., *Flückiger et al.*, 2008]

$$Y_i(P, h) = \sum_j \int \int A_i(E, \theta) \cdot F_{i,j}(P, h, E, \theta)\, dE\, d\Omega \qquad (2)$$

where $A_i(E,\theta)$ is the geometrical detector area times the registration efficiency, $F_{i,j}$ is the differential flux of secondary particles of type j (neutrons, protons, muons, and pions) for the primary particle of type i, E is the secondary particle's energy, θ is the angle of incidence of secondaries. Thus, the yield function consists of two parts. One is the cascade in the Earth's atmosphere that produces secondary particles, viz. the term F in equation (2), and the other is the response

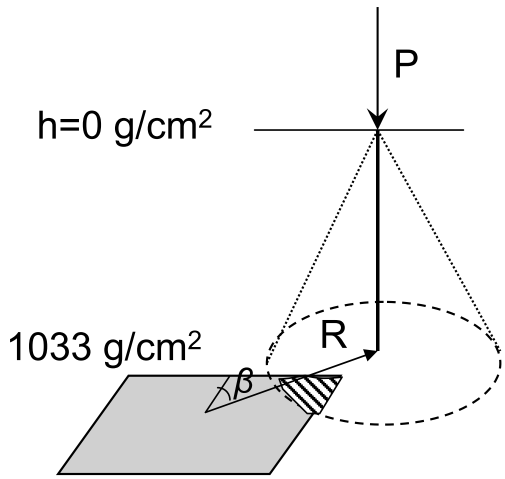

Figure 1. A scheme illustrating the way to calculate the geometrical factor G of the NM effective size. The gray shape represents the physical size of the NM at the sea level, while the dashed line corresponds to the lateral extend of the hadronic component of an atmospheric cascade started on the top of the atmosphere. The hatched area denotes that secondaries of the cascade hit the detector. The scheme illustrates a general situation when a cascade, initiated by a primary CR particle with rigidity P impinging on the top of the atmosphere, has its axis at distance R and azimuth angle β from the NM center.

of the detector itself, the A-term, to these secondary particles, mainly neutrons and protons. We will consider these two parts separately.

[9] As the standard NM, we consider here a sea-level 6NM64 [*Stoker et al*., 2000; *Moraal et al*., 2000].

2.1. CR-induced Atmospheric Cascade

[10] As the first step, we obtained the atmospheric flux of various secondary CR particles, as denoted by term F in equation (2). The computations were performed on the basis of simulations with PLANETOCOSMICS code [*Desorgher et al*., 2005], based on GEANT-4 [*Agostinelli et al*., 2003], similar to [*Flückiger et al*., 2008; *Matthiä et al*., 2009]. The main contribution to the NM count rate is due to secondary neutrons and protons [*Hatton*, 1971; *Clem and Dorman*, 2000; *Dorman*, 2004]. As an input for the simulations, we used primary particles (protons and α-particles) with the fixed energy ranging from 100 MeV/nucleon to 1 TeV/nucleon that impinges the top of the atmosphere with a given angle of incidence. A realistic curved atmospheric model NRLMSISE2000 [*Picone et al*., 2002] was employed for the simulations. The computations were normalized per one primary particle. We recorded secondary particles (protons and neutrons separately) with energy within the energy bin $E_n \pm \Delta E$ that cross a given horizontal level at the atmospheric depth 1033 g/cm^2, corresponding to the sea level. The result of simulations corresponds to the flux of secondary neutrons and protons with given energy across a horizontal unit area.

[11] We explicitly consider CR particles heavier than protons, primarily α-particles. After the first inelastic collision in the atmosphere, the primary nucleus is disintegrated and is effectively represented by nucleons, so that from the point of view of the atmospheric cascade at the sea level, e.g., an α-particle is almost equivalent to four protons with the same energy per nucleon [*Engel et al*., 1992]. However, because of the lower Z/A ratio, heavier species are less modulated by both geomagnetic field and in the heliosphere. Therefore, heavier species should be considered explicitly, not through scaling protons. On the other hand, α-particles are representative for all GCR species heavier than proton [*Webber and Higbie*, 2003; *Usoskin et al*., 2011], as their rigidity-to-energy per nucleon ratio, and thus the modulation/shielding effect, is nearly the same, as well as their cascade initiation ability expressed per nucleon with the same energy. The assumption that all the heavier species can be effectively represented by α-particles via simple scaling might lead to an additional uncertainty in the middle-upper atmosphere above the height of about 15 km, but it works well in the lower atmosphere. It has been numerically tested that nitrogen, oxygen, and iron are very similar to α-particle (scaled by the nucleonic number with the same energy per nucleon) in the sense of the atmospheric cascade at the sea level [e.g., *Usoskin et al*., 2008; *Mishev and Velinov*, 2011].

[12] Since the contribution of obliquely incident primaries is important [*Clem et al*., 1997], in particular for the analysis of solar energetic particle events [*Cramp et al*., 1997; *Vashenyuk et al*., 2006], we simulated cascades induced by protons with various angles of incidence on the top of the atmosphere.

[13] The difference in the fluxes of secondary particles at the sea level between vertical and 15° inclined primary protons is not significant, but the secondary particle flux decreases with further increase of the incident angle, as the mass overburden increases, resulting on NM yield function decrease. In the forthcoming results, we consider isotropic (within 2π steradian) flux of incoming primary GCR.

[14] As many as 10^6 cascades were simulated for each energy point and for each type of primary particle (proton or α). The atmospheric cascade simulation is explicitly performed with PLANETOCOSMICS code for primary α-particles in the energy range below 10 GeV/nucleon using the same assumptions and models as for protons. For the energy above 10 GeV/nucleon, we substitute an α-particle with four nucleons (protons), similar to recent works [*Usoskin and Kovaltsov*, 2006; *Mishev and Velinov*, 2011].

2.2. NM Registration Efficiency

[15] As the detector's own registration efficiency, denoted as term A in equation (2), we apply the results by *Clem and Dorman* [2000] in an updated version [J. Clem and B. Gvozdevsky, private communications, 2011–2012].

[16] We noted that there is a process, which has not been accounted for in previous studies, that increases the effective area of a NM for more energetic CRs, compared to the physical area of the detector. This is the finite lateral extension of the atmospheric cascades, which is typically neglected when considering the NM yield function. It is normally assumed that only cascades with axes hitting the physical detector's body cause response. However, even cascades which are outside the detector may contribute to the count rate, as illustrated in Figure 1. The size of a 6NM64 monitor is about 2×6 m, and a typical size of the secondary particle flux spatial span (full width at half magnitude) at the sea level is several meters.

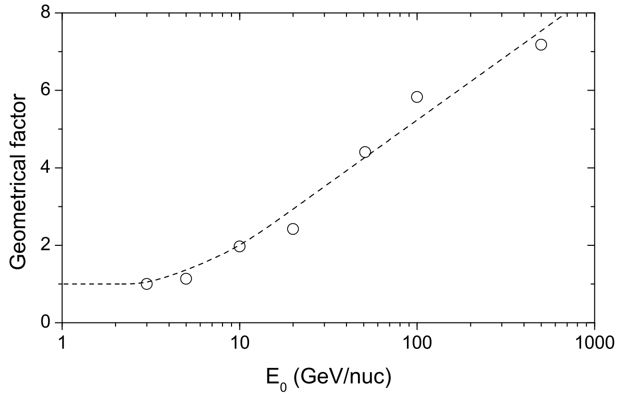

Figure 2. The effective geometrical factor G (equation (4)) as function of the primary CR particle's energy for protons. Dots are the results of the Monte-Carlo simulations and the dashed line is the used approximation.

[17] We have performed the full Monte-Carlo simulation of this effect in the following way. We simulated cascades, caused by a primary CR particle with rigidity P, whose axis lies at the distance R and azimuth angle β from the center of the NM (Figure 1), and calculated the number $N(R,\beta,P)$ of secondary hadrons with energy above 1 MeV hitting the detector (hatched area in the Figure). This step was repeated 10^5 time for each set of R and P with the uniform random azimuthal distribution so that it includes averaging over the angle β. As an example, $N \approx 0.01$ is found for a 3 GeV proton, vertically impinging on the top of the atmosphere above the center of NM. We note that this energy corresponds to the effective energy of a polar NM, viz. to the maximum of the integrand of equation (1). Then, the weight of such a remote cascade was calculated as

$$w(R,P) = \min[N(R,P);1]. \tag{3}$$

[18] This weighting takes into account that a standard NM has a large dead time (about 2 ms) which cuts off the multiplicity of the counts [*Stoker et al.*, 2000]. In other words, if many secondary particles hit a NM counter, there is still only one count, and all the subsequent multiple counts are cut off by the dead time of the detector. Thus, we assume that, if several secondary particles from the same cascade hit the detector within the dead time, the number of counts is not increased. The considered effect will be greater for NMs with short dead time to study multiplicities. Then, the effective geometrical factor of the NM with the account for this effect is calculated as

$$G(P) = \frac{2\pi}{S_{\rm NM}} \int_0^\infty R \cdot w(R,P) \cdot dR \tag{4}$$

where $S_{\rm NM}$ is the geometrical area of a 6NM64. The effective geometrical factor G is shown in Figure 2 as dots. One can see that above the energy of 5 GeV, it is a logarithmically growing function of energy. For further calculations, we used an approximation shown as the dashed line in the figure. We note that this geometrical factor is slightly greater for smaller NMs and smaller for bigger NMs.

[19] Then, the definition of the NM yield function becomes as the following (cf. equation (2))

$$Y_i(P,h) = G(P)\sum_i \int\int A_i(E,\theta) \cdot F_{i,j}(P,h,E,\theta)\, dE\, d\Omega \tag{5}$$

2.3. The NM Yield Function

[20] Here we present the results for the new computations of the yield function of a standard NM, applying also the earlier neglected correction of the geometrical factor of a NM. The tabulated values are given in Table 1. Figure 3 presents the normalized yield functions of the standard sea-level 6NM64 NM computed for isotropically incident CR protons and α-particles.

[21] One can see that the yield function for protons (Figure 3A) is close to earlier computations (except for that by *Clem and Dorman* [2000]) in the lower energy range below about 10 GeV energy, but is greater than those in the higher energy range. The latter is due to the geometrical correction factor (Figure 2). The agreement in the lower

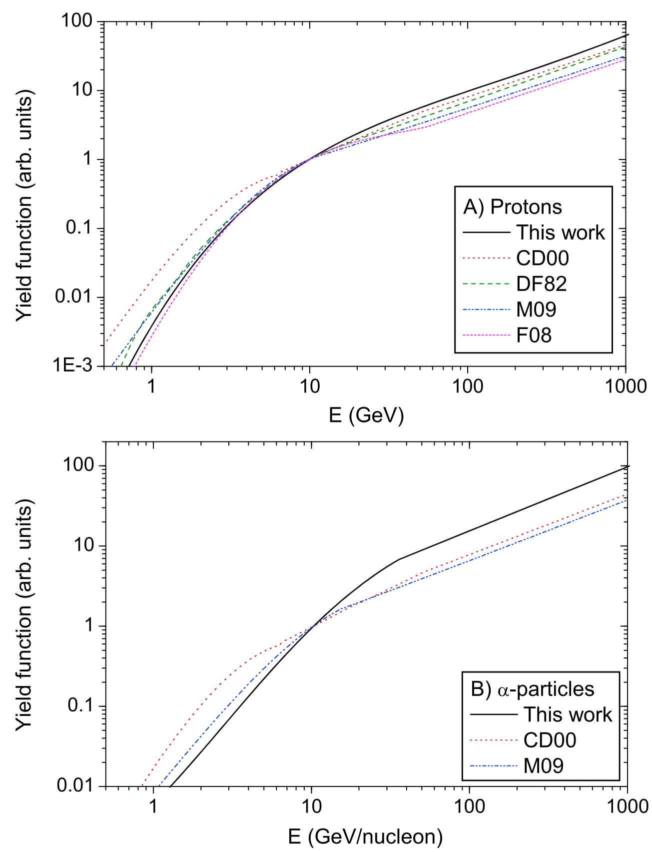

Figure 3. The normalized (to unity at 10 GeV) yield function of the standard sea-level NM64 neutron monitor, calculated for CR protons (panel A) and α-particles (panel B). Different curves correspond to different models: CD00 [*Clem*, 1999; *Clem and Dorman*, 2000]; DF82 [Debrunner et al., 1982]; M09 [*Matthiä*, 2009; *Matthiä et al.*, 2009]; F08 [*Flückiger et al.*, 2008]. When the high-energy part (above 50–100 GeV) is not available from the original works, it has been extrapolated using a power law.

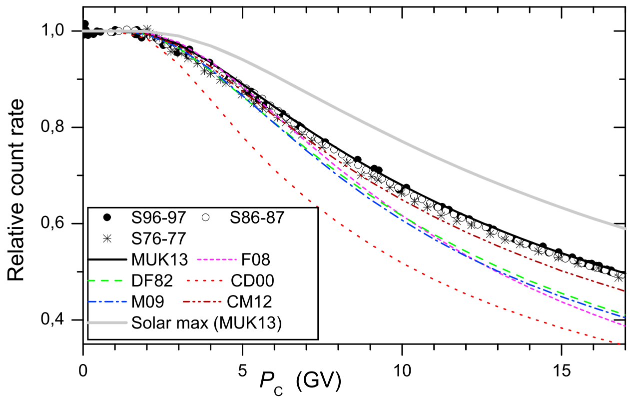

Figure 4. Latitude surveys. Experimental data are depicted by symbols, while computed profiles are given as curves. The data include surveys in 1996–1997 [*Villoresi et al.*, 2000, filled dots], 1986–1987 [*Moraal et al.*, 1989, open dots], and 1976–77 [*Potgieter et al.*, 1979, asterisks]. The models are: this work [MUK13], [*Flückiger et al.*, 2008, F08], [*Debrunner et al.*, 1982, DF82], [*Clem*, 1999; *Clem and Dorman*, 2000, CD00], [*Matthiä et al.*, 2009, M09], [*Caballero-Lopez and Moraal*, 2012, CM12]. All count rates are normalized to the polar region. The gray curve depicts a survey calculated (using this model) for a solar maximum with φ = 1200 MV.

energy range is particularly good with those [*Flückiger et al.*, 2008; *Matthiä et al.*, 2009] based on the same GEANT-4 Monte-Carlo tool as our work. The yield function for α-particles has larger differences with respect to the earlier works, particularly [*Clem and Dorman*, 2000] who used FLUKA Monte-Carlo package.

3. Verification of the Model: Latitude Survey

[22] As discussed above, a latitude survey, viz. change of the count rate of a standard NM surveying over latitudes, provides a direct test to the computation of the NM count rate and thus to the yield function. Surveys are usually performed onboard a ship cruising between equatorial and polar regions. Since such a cruise may take several months, they are made during the times of solar minimum in order to secure the least temporal variability of the CR flux so that all the changes in the surveying NM are caused by the changing geomagnetic shielding along the route [*Moraal et al.*, 2000]. Here we consider three surveys, shown in Figure 4, performed at consecutive solar minima in 1976–1977 [*Potgieter et al.*, 1979], 1986–1987 [*Moraal et al.*, 1989], and 1996–1997 [*Villoresi et al.*, 2000]. The heliospheric conditions were similar during all the three surveys, with the modulation parameter being φ = 400 ± 20 MV [*Usoskin et al.*, 2011]. Accordingly, we will consider all the three surveys as one. As the GCR spectrum, we consider the force-field approximation with the fixed modulation parameter φ = 400 MV.

[23] All the earlier theoretically calculated NM yield functions were unable to reproduce the observed latitude surveys [*Clem and Dorman*, 2000; *Caballero-Lopez and Moraal*, 2012]. In order to test the yield functions, we have calculated the results of the latitude survey, predicted by these models, by applying equation (1) and using measured or modelled spectrum of CRs [see methodology in *Usoskin et al.*, 2005]. Here we consider the parametrization of the GCR energy spectrum [*Usoskin et al.*, 2005] via the modulation potential φ and the local interstellar spectrum according to *Burger et al.* [2000]. This parametrization is widely used in many applications and has been validated by comparisons with direct balloon- and space-borne GCR measurements [*Usoskin et al.*, 2011; *PAMELA collaboration et al.*, 2012]. We note that there is an uncertainty in the exact shape of the GCR spectrum, and many other approximations exist [e.g., *Herbst et al.*, 2010, and references therein]. When applying other GCR spectral models, the results presented here would be slightly changed of the order of 10%. Computations were done separately for both protons and α-particles, which effectively include also heavier CR species, similar to *Usoskin et al.* [2011]. Only CD00, M09, and the present work provide the NM yield function for primary α-particles. In all other cases, we applied the proton yield function also for α-particles. The results of the computations are shown as curves in Figure 4. One can see that the lowest curve for the CD00 yield function overestimates the ratio between pole and equator by roughly a factor of two. Other theoretical curves (DF82, F08, and M09) lie close to each other but about 20% lower than the observed latitude survey. The CM12 curve is based on an ad-hoc empirical yield function designed to fit the latitude survey. Therefore, it is expected that it appears close to the measured profile. A small 7–10% discrepancy is caused by the different energy spectra of GCR used here and by *Caballero-Lopez and Moraal* [2012]. We note that, provided the same spectral shape is used, the CM12 result must lie on the observed latitude survey curve by definition. The theoretical yield function presented in this work (MUK13) precisely reproduces the observed latitude survey, without any ad-hoc calibration or adjustment. We note that our present yield function, but without the geometrical correction (section 2.2), yields the results very similar to that by CD00. Thus, the account for the geometrical correction fully resolves the problem of the NM yield function being in disagreement with the experimental latitude surveys of NMs.

4. Conclusions

[24] We have presented here a newly computed yield function of the standard sea-level NM 6NM64, separately for primary protons and α-particles, the latter representing also heavier species of CRs [*Webber and Higbie*, 2003]. The computations have been done using the GEANT-4 tool PLANETOCOSMICS and a realistic atmospheric model. For the first time, an important but previously neglected effect of the geometrical correction of the NM size, related to the finite lateral expansion of the CR-induced atmospheric cascade, is considered. This correction enhances the relative impact of higher-energy CRs (energy above 5–10 GeV/nucleon) in the NM count rate leading to weaker dependence of GCR on the geomagnetic shielding. This improves the situation with the long-standing problem of disagreement between the theoretically calculated spatial variability of CRs over the globe and the experimental latitude surveys. The NM yield function, corrected for this geometrical factor, appears perfectly consistent with the experimental latitude surveys

of NMs performed during three consecutive solar minima in 1976–1977, 1986–1987, and 1996–1997. On the other hand, this geometrical correction does not affect analysis of events in solar energetic particles whose energy is usually below a few GeV.

[25] Thus, we provide a new yield function of the standard sea-level NM 6NM64 that is validated versus confrontation with experimental data and can be applied in detailed studies of CR variability on different spatial and temporal scales.

[26] **Acknowledgments.** This work was partly funded from the European Union's 7-th Framework Program (FP7/2007–2013) under grant agreement N 262773 (SEPServer), by the Academy of Finland and by the Väisälä foundation. We acknowledge the high-energy division of Institute for Nuclear Research and Nuclear Energy - Bulgarian Academy of Sciences for the computational time. The authors warmly acknowledge John Clem and Boris Gvozdevsky for the updated information concerning the NM registration efficiency. We acknowledge also Vladimir Makhmutov for information related to PLANETOCOSMICS simulations, as well as Eduard Vashenuyk and Yury Balabin for fruitful discussions concerning GLE analysis. G.A. Kovaltsov was partly supported by the Program No. 22 of presidium of Russian Academy of Sciences.

References

Agostinelli, S., et al. (2003), Geant4-a simulation toolkit, *Nucl Instr. Meth. Phys. Res. A*, *506*, 250–303.

Ahluwalia, H. S., M. M. Fikani, and R. C. Ygbuhay (2010), Rigidity dependence of 11 year cosmic ray modulation: Implication for theories, *J. Geophys. Res.*, *115*, A07101, doi:10.1029/2009JA014798.

Bazilevskaya, G. A., et al. (2008), Cosmic ray induced ion production in the atmosphere, *Space Sci. Rev.*, *137*, 149–173, doi:10.1007/s11214-008-9339-y.

Burger, R., M. Potgieter, and B. Heber (2000), Rigidity dependence of cosmic ray proton latitudinal gradients measured by the ulysses spacecraft: Implications for the diffusion tensor, *J. Geophys. Res.*, *105*, 27,447–27,456.

Caballero-Lopez, R., and H. Moraal (2012), Cosmic-ray yield and response functions in the atmosphere, *J. Geophys. Res.*, *117*, A12103, doi:10.1029/2012JA017794.

Clem, J. (1999), Atmospheric Yield Functions and the Response to Secondary Particles of Neutron Monitors, in *26th Internat. Cosmic Ray Conf., Salt Lake City*, vol. 7, pp. 317–311.

Clem, J., and L. Dorman (2000), Neutron monitor response functions, *Space Sci. Rev.*, *93*, 335–359, doi:10.1023/A:1026508915269.

Clem, J. M., J. W. Bieber, P. Evenson, D. Hall, J. E. Humble, and M. Duldig (1997), Contribution of obliquely incident particles to neutron monitor counting rate, *J. Geophys. Res.*, *102*, 26,919–26,926, doi:10.1029/97JA02366.

Cramp, J. L., M. L. Duldig, E. O. Flückiger, J. E. Humble, M. A. Shea, and D. F. Smart (1997), The October 22, 1989, solar cosmic ray enhancement: An analysis of the anisotropy and spectral characteristics, *J. Geophys. Res.*, *102*, 24,237–24,248, doi:10.1029/97JA01947.

Debrunner, H., and E. Å. Brunberg (1968), Monte Carlo calculation of the nucleonic cascade in the atmosphere, *Can. J. Phys. Suppl.*, *46*, 1069–1072.

Debrunner, H., E. Flückiger, and J. Lockwood (1982), Specific yield function S(P) for a neutron monitor at sea level, paper presented, in *8th Europ. Cosmic ray Symp.*, Rome, Italy.

Desorgher, L., E. O. Flückiger, M. Gurtner, M. R. Moser, and R. Bütikofer (2005), Atmocosmics: a Geant 4 Code for Computing the Interaction of Cosmic Rays with the Earth's Atmosphere, *Int. J. Modern Phys. A*, *20*, 6802–6804, doi:10.1142/S0217751X05030132.

Dorman, L. (2004), *Cosmic Rays in the Earth's Atmosphere and Underground*, pp. 216–242, Kluwer Academic Publishers, Dordrecht.

Engel, J., T. K. Gaisser, P. Lipari, and T. Stanev (1992), Nucleus-nucleus collisions and interpretation of cosmic-ray cascades, *Phys. Rev. D*, *46*, 5013–5025, doi:10.1103/PhysRevD.46.5013.

Flückiger, E. O., et al. (2008), A parameterized neutron monitor yield function for space weather applications, in *30th Proc. Internat. Cosmic Ray Conf. 2007*, vol. 1, edited by R. Caballero, J. D'Olivo, G. Medina-Tanco, L. Nellen, F. Sánchez, and J. Valdés-Galicia, pp. 289–292, Universidad Nacional Autónoma de México, Mexico City, Mexico.

Hatton, C. J. (1971), The Neutron Monitor, in *Processes in Elementary Particle and Cosmic Ray Physics*, edited by J. G. Wilson, and S. A. Wouthuysen, pp. 3–100, North-Holland Publ. Comp., Amsterdam-London.

Heck, D. (2006), Low-energy hadronic interaction models, *Nucl. Phys. B Proc. Suppl.*, *151*, 127–134, doi:10.1016/j.nuclphysbps.2005.07.024.

Herbst, K., A. Kopp, B. Heber, F. Steinhilber, H. Fichtner, K. Scherer, and D. Matthiä (2010), On the importance of the local interstellar spectrum for the solar modulation parameter, *J. Geophys. Res.*, *115*, D00I20, doi:10.1029/2009JD012557.

Krüger, H., H. Moraal, J. W. Bieber, J. M. Clem, P. A. Evenson, K. R. Pyle, M. L. Duldig, and J. E. Humble (2008), A calibration neutron monitor: Energy response and instrumental temperature sensitivity, *J. Geophys. Res.*, *113*, A08101, doi:10.1029/2008JA013229.

Matthiä, D. (2009), The Radiation Environment in the Lower Atmosphere: A Numerical Approach, Ph.D. thesis, Christian-Albrechts-Universität zu Kiel.

Matthiä, D., B. Heber, G. Reitz, M. Meier, L. Sihver, T. Berger, and K. Herbst (2009), Temporal and spatial evolution of the solar energetic particle event on 20 January 2005 and resulting radiation doses in aviation, *J. Geophys. Res.*, *114*, A08104, doi:10.1029/2009JA014125.

Mishev, A. L., and P. I. Y. Velinov (2011), Normalized ionization yield function for various nuclei obtained with full Monte Carlo simulations, *Adv. Space Res.*, *48*, 19–24, doi:10.1016/j.asr.2011.02.008.

Moraal, H., M. S. Potgieter, P. H. Stoker, and A. J. van der Walt (1989), Neutron monitor latitude survey of cosmic ray intensity during the 1986/1987 solar minimum, *J. Geophys. Res.*, *94*, 1459–1464, doi:10.1029/JA094iA02p01459.

Moraal, H., A. Belov, and J. M. Clem (2000), Design and co-Ordination of Multi-Station International Neutron Monitor Networks, *Space Sci. Rev.*, *93*, 285–303, doi:10.1023/A:1026504814360.

PAMELA collaboration, I. G. Usoskin, and G. A. Kovaltsov (2012), On the validity of force-field approximation for galactic cosmic ray spectrum during forbush decreases, in *Procs. 23rd European Cosmic Ray Symp.*, p. ID 528, Moscow.

Picone, J. M., A. E. Hedin, D. P. Drob, and A. C. Aikin (2002), NRLMSISE-00 empirical model of the atmosphere: Statistical comparisons and scientific issues, *J. Geophys. Res.*, *107*(A12), 1468, doi:10.1029/2002JA009430.

Potgieter, M. S. (1998), The Modulation of Galactic Cosmic Rays in the Heliosphere: Theory and Models, *Space Sci. Rev.*, *83*, 147–158.

Potgieter, M., B. Raubenhaimer, and P. Stoker (1979), The latitude distribution of cosmic rays at sea level during the recent period of minimum solar activity, in *16th Internat. Cosmic Ray Conf., Kyoto*, vol. 4, pp. 352–357.

Shea, M. A., and D. F. Smart (2000), Fifty Years of Cosmic Radiation Data, *Space Sci. Rev.*, *93*, 229–262, doi:10.1023/A:1026500713452.

Simpson, J. A. (1958), Cosmic radiation neutron intensity monitor, in *Annals of the Int. Geophysical Year IV, Part VII*, Pergamon Press, London, pp. 351.

Smart, D. F., M. A. Shea, A. J. Tylka, and P. R. Boberg (2006), A geomagnetic cutoff rigidity interpolation tool: Accuracy verification and application to space weather, *Adv. Space Res.*, *37*, 1206–1217, doi:10.1016/j.asr.2006.02.011.

Stoker, P. H., L. I. Dorman, and J. M. Clem (2000), Neutron Monitor Design Improvements, *Space Sci. Rev.*, *93*, 361–380, doi:10.1023/A:1026560932107.

Usoskin, I. G., and G. A. Kovaltsov (2006), Cosmic ray induced ionization in the atmosphere: Full modeling and practical applications, *J. Geophys. Res.*, *111*, D21206, doi:10.1029/2006JD007150.

Usoskin, I. G., K. Alanko-Huotari, G. A. Kovaltsov, and K. Mursula (2005), Heliospheric modulation of cosmic rays: Monthly reconstruction for 1951–2004, *J. Geophys. Res.*, *110*, A12108, doi:10.1029/2005JA011250.

Usoskin, I., L. Desorgher, P. Velinov, M. Storini, E. Flückiger, R. Bütikofer, and G. Kovaltsov (2008), Solar and galactic cosmic rays in the earth's atmosphere, in *COST 724 final report: Developing the scientific basis for monitoring, modelling and predicting Space Weather*, edited by J. Lilensten, A. Belehaki, M. Messerotti, R. Vainio, J. Watermann, and S. Poedts, pp. 124–132, COST Office, Luxemburg.

Usoskin, I. G., G. A. Bazilevskaya, and G. A. Kovaltsov (2011), Solar modulation parameter for cosmic rays since 1936 reconstructed from ground-based neutron monitors and ionization chambers, *J. Geophys. Res.*, *116*, A02104, doi:10.1029/2010JA016105.

Vashenyuk, E. V., Y. V. Balabin, J. Perez-Peraza, A. Gallegos-Cruz, and L. I. Miroshnichenko (2006), Some features of the sources of relativistic particles at the Sun in the solar cycles 21 23, *Adv. Space Res.*, *38*, 411–417, doi:10.1016/j.asr.2005.05.012.

Villoresi, G., L. I. Dorman, N. Iucci, and N. G. Ptitsyna (2000), Cosmic ray survey to Antarctica and coupling functions for neutron component near solar minimum (1996–1997) 1. Methodology and data quality assurance, *J. Geophys. Res.*, *105*, 21,025–21,034, doi:10.1029/2000JA900048.

Webber, W., and P. Higbie (2003), Production of cosmogenic be nuclei in the earth's atmosphere by cosmic rays: Its dependence on solar modulation and the interstellar cosmic ray spectrum, *J. Geophys. Res.*, *108*(A9), 1355, doi:10.1029/2003JA009863.

Erratum

In the originally published version of this paper, the values of Y_α (the last column of Table 1) in the first five lines were erroneously divided by a factor of four. (Other values in the table remain unaltered.) The corrected Table 1 is presented here. This version may be considered the authoritative version of record.

Table 1. Yield Function (in Units of [m^2 sr]) of the Standard 6NM64 Sea-Level Neutron Monitor for the Primary Protons (Columns 2–3) and α-Particles (Columns 5–6), Per Nucleon of the Primary Particle

Protons			α-Particles		
P (GV)	E_p (GeV)	Y_p	P (GV)	E_α (GeV/nuc)	Y_α
0.7	0.232	$7.26 \cdot 10^{-9}$			
1	0.433	$8.46 \cdot 10^{-6}$	3.38	1	$1.54 \cdot 10^{-3}$
2	1.27	$1.21 \cdot 10^{-3}$	5.55	2	$8.64 \cdot 10^{-3}$
3	2.21	$5.42 \cdot 10^{-3}$	7.64	3	$1.72 \cdot 10^{-2}$
4	3.17	$9.43 \cdot 10^{-3}$	9.69	4	$2.91 \cdot 10^{-2}$
5	4.15	0.02	11.7	5	$4.72 \cdot 10^{-2}$
10	9.11	0.109	21.8	10	$8.37 \cdot 10^{-2}$
20	19.1	0.229	41.8	20	0.215
50	49.1	0.59	100	49.1	0.59
100	99.1	0.992	200	99.1	0.992
500	499.1	3.35	1000	499.1	3.35
1000	999.1	6.67	2000	999.1	6.67